Gadolinium-Based Nanoparticles Combined With Checkpoint Blockade Amplify Radiation-Induced Abscopal Effect And Cancer Immunotherapy

Huijuan Song（✉ songhuijuan@irm-cams.ac.cn）

Chinese Academy of Medical Sciences & Peking Union Medical College

Ningning He

CAMS IRM: Chinese Academy of Medical Sciences & Peking Union Medical College Institute of Radiation Medicine

Chang Xu

CAMS IRM: Chinese Academy of Medical Sciences & Peking Union Medical College Institute of Radiation Medicine

Yan Wang

CAMS IRM: Chinese Academy of Medical Sciences & Peking Union Medical College Institute of Radiation Medicine

Liqing Du

CAMS IRM: Chinese Academy of Medical Sciences & Peking Union Medical College Institute of Radiation Medicine

Yang Liu

CAMS IRM: Chinese Academy of Medical Sciences & Peking Union Medical College Institute of Radiation Medicine

Qin Wang

CAMS IRM: Chinese Academy of Medical Sciences & Peking Union Medical College Institute of Radiation Medicine

Kaihua Ji

CAMS IRM: Chinese Academy of Medical Sciences & Peking Union Medical College Institute of Radiation Medicine

Jinhan Wang

CAMS IRM: Chinese Academy of Medical Sciences & Peking Union Medical College Institute of Radiation Medicine

Manman Zhang

CAMS IRM: Chinese Academy of Medical Sciences & Peking Union Medical College Institute of Radiation Medicine

Yeqing Gu

CAMS IRM: Chinese Academy of Medical Sciences & Peking Union Medical College Institute of Radiation Medicine

Yumin Zhang

CAMS IRM: Chinese Academy of Medical Sciences & Peking Union Medical College Institute of Radiation Medicine

Weiwei Wang

Chinese Academy of Medical Sciences & Peking Union Medical College Institute of Biomedical Engineering

Olivier Tillement

University of Lyon: Universite de Lyon

Li Feng

Shandong Qianfoshan Hospital

Qiang Liu

CAMS IRM: Chinese Academy of Medical Sciences & Peking Union Medical College Institute of Radiation Medicine

---

Research Article

Abstract

Both immunotherapy checkpoint blocking and radiotherapy used alone in solid tumors show limited anticancer effect, due to the insufficient T cells infiltration and rarely elicited systemic immune responses.

Methods: AGuIX has recently been developed for magnetic resonance imaging-guided radiotherapy and proven to act as an efficient radiosensitizer. In order to further improve the efficiency of tumor treatment, a unique synergistic strategy based on Gadolinium-based nanoparticles-AGuIX mediated radiotherapy and immunotherapy checkpoint blocking was developed for B16 tumor therapy in the present study. Clone formation, cell apoptosis and immunofluorescence were performed to detect the radiosensitization effect of AGuIX nanoparticles. The therapeutic effect was validated in both abscopal and metastasis tumor models, and analyzed the synergistic mechanism *in vivo*.

Results: AGuIX as a radiosensitizer exacerbated radiation-induced DNA damage, cell cycle arrest and apoptosis on B16 cells. More importantly, it could efficiently induce the immunogenic cell death (ICD) of irradiated B16 tumor cells, and consequently triggered the maturation of dendritic cells (DCs) and activated systemic T-cell responses. Combining AGuIX-mediated radiotherapy with programmed cell death protein 1 (PD1) blocking demonstrated excellent synergistic therapeutic effects in both abscopal and metastasis tumor models by a significant increase in the infiltration of effector $CD8^+$ T cells and effectively alleviating the immunosuppressive microenvironment, including regulatory T cells (Tregs) and myeloid-derived suppressor cells (MDSCs) in tumors.

Conclusion: Our findings indicate that this combination therapy provided a new and powerful immunotherapy model to achieve durable anti-tumor responses, which is likely to be a promising comprehensive treatment strategy for cancer treatment.

Background

Radiotherapy (RT) is a classic and irreplaceable antitumor strategy that has been extensively used in clinical cancer therapy [1, 2]. DNA double strand break (DSB) is the main mechanism effectively induces growth arrest and apoptosis of tumor cells irradiated by γ-rays or X-rays [3]. Therefore, some radiosensitizers that can aggravate DNA breakage, inhibit DNA repair and improve hypoxic tumor microenvironment are extensively studied to maximize the radiotherapeutic efficacy [4, 5]. Meanwhile, it should be pointed out that the appropriate dose of RT could activate the immune response and thus amplify its anti-tumor efficiency, which provides an opportunity for combination with immunotherapy [6, 7]. RT can cause tumor cells to immunogenic cell death (ICD), and release tumor-associated antigens (TAAs) as well as damage associated molecular patterns (DAMPs) [8, 9]. Therefore, irradiated tumor cells may potentially serve as an "in situ vaccine" to activate the classic innate and adaptive anti-tumor immune responses [10]. However, a large amount of clinical and preclinical evidence has been suggested that the immunogenicity of tumor cells caused by RT alone is relatively weak, and it is not enough to be presented by antigen presenting cells (APCs) to trigger anti-tumor immune responses[11, 12]. Moreover,

high-dose RT/not fractionated may also potentially produce immunosuppressive effects, because the chemokines and cytokines (such as IL-1, IL-6, IL-10 and TGF-β) produced by RT also attract the recruitment of immunosuppressive cells, including tumor-associated macrophages (TAMs), myeloid-derived suppressor cells (MDSCs), regulatory T cells (Tregs)[13, 14]. Therefore, it is urgent to find a radiosensitizer to reduce the radiation dose while ensuring the efficiency of RT, so as to eliminate the suppression of the immune system caused by high-dose RT.

Nanoparticles of heavy metals such as gold and HfO2 have been proved to be promising radiotherapy sensitizers, which can produce more ROS to exacerbate DNA breakage [15]. AGuIX nanoparticles, a kind of heavy-metal nanoparticles, were comprised of polysiloxane and surrounded by gadolinium chelates, which have also been shown to be effective radiosensitizers through increasing radiation-induced DNA damage, cell cycle arrest, and cell apoptosis [16]. The mechanism may be related to two major pathways of affecting the DNA damage repair in tumor cells: homologous recombination (HR) and non-homologous end junction (NHEJ) [17]. The research on AGuIX nanoparticles involves head and neck cancer, lung cancer and brain cancer. Recently, combined with RT for the treatment of brain metastasis has entered a phase III clinical trial [18]. Through the use of tumor-targeted radiation enhancer-AGuIX, we can reduce the radiation dose while maintaining enough ionizing damage to the tumor, which can further alleviate the side effects on the surrounding normal tissues. Therefore, AGuIX nanoparticles-mediated low-dose RT is expected to magnify tumor ICD and enhance the anti-tumor immune responses.

Immune checkpoint inhibitors are clinically effective against a variety of tumors, showing remarkable progress and hope [19]. However, they are only effective for some tumor patients, and the overall effective rate is only about 20-30%. They can relieve the inhibition of T cell activation, but if there are no T cells inside/near the tumors, it is difficult for such drugs to exert efficacy [20]. Therefore, although immune checkpoint inhibitors are a major breakthrough in tumor immunotherapy, their success is expected to be extended to other treatment modalities. Among them, RT and chemotherapy show certain immunomodulatory potential by inducing ICD, releasing tumor antigens and promoting T cells migration and infiltration to the tumor site, which actively seek to combine with checkpoint blocking immunotherapy to break drug resistance and immune escape in tumors [21–23].

Therefore, here we report a therapeutic strategy to trigger systemic immune responses against B16 tumors in mouse models by combining AGuIX-mediated RT with checkpoint blocking therapy. Clonogenic assays and intracellular ROS measurements showed that AGuIX displayed radioenhancing efficiency. We also demonstrated in vitro and in vivo that AGuIX-mediated low-dose RT could cause ICD of tumor cells, release DAMPs including calreticulin (CRT) and high mobility group protein B-1(HMGB1), activate antigen-presenting cells, and trigger tumor-specific T cells response. On the other hand, AGuIX-mediated low-dose RT combined with an anti-PD1 antibody also promoted effector T cells recruitment, infiltration, removed Tregs and MDSCs from the tumors by secreted chemokines and cytokines, and realized the remodeling of the tumor immune microenvironment. Finally, AGuIX-mediated low-dose RT coordinated with an anti-PD1 antibody could not only inhibit local tumors, but also eradicate distant tumors depending on the systemic anti-tumor immunity in a bilateral B16 melanoma and pulmonary metastasis

models, suggesting this strategy enhanced the abscopal effect of RT (Scheme 1). When selectively depleting CD4 and CD8 T cells, the anti-tumor effects produced by AGuIX-mediated RT were significantly weakened, further confirming that the collaborative treatment modality regulated the immune system and strongly relied on T cells. Therefore, we profile the underlying mechanisms of this combination immunotherapy was the increase of effector T cells and reprogramming of immunosuppressive microenvironment in tumors.

Results And Discussion

Synthesis and characterization of AGuIX nanoparticles

In view of the fact that heavy metal nanoparticles have been used as a promising radiosensitizer, we designed and developed a new efficient gadolinium-based theranostic agent-AGuIX for MRI-guided RT [24]. Pre-clinical studies had also demonstrated AGuIX particles could act as efficient radiosensitizers, and their significant therapeutical effect on many types of ectopic and orthotopic transplanted tumors by intratumoral injection or intravenous administration [25]. In order to produce a sufficient number of nanoparticles for in vivo applications and further potential clinical applications, a large-scale top-down synthesis method had been established [26]. Their chemical composition was analyzed by inductively coupled plasma mass spectrometry (ICP-MS). The elemental composition of Gd, Si, N and C was shown in in Figure 1A. AGuIX were composed of 12.7% Gd (w/w), 9.1% Si (w/w), 29.4% C (w/w) and 7.5% N (w/w). HPLC measurements indicated the purity of the colloidal solution was excellent, and the Gd concentration stayed approximately equal to 15 mmol (Figure 1B). Dynamic Light Scattering (DLS) displayed hydrodynamic diameter of AGuIX nanoparticles was 3.1 ± 1 nm, and transmission electron microscopy (TEM) imaging exhibited the morphology was spherical with a diameter of nearly 3 nm (Figure 1C). Generally speaking, silica particles with hydrodynamic diameters between 3 and 7 nm combined reasonable circulation lifetimes and efficient renal clearance [27], so AGUIX should also have these two advantages. Zeta potential is usually used to evaluate or predict the physical stability of particle dispersion systems. Generally, the higher the absolute value of Zeta potential, the greater the electrostatic repulsion between particles, and the better the physical stability [28]. Figure 1D demonstrates the high colloidal stability of AGuIX nanoparticles. Their excellent physical and chemical properties will undoubtedly promote major advances in the therapeutic and diagnostic approach of radiotherapy.

AGuIX nanoparticles increased the radiosensitivity on B16 tumor cells.

At our previous work, we had confirmed the radiosensitization effect of AGuIX nanoparticles on H1299 and A549 NSCLC cells [17]. Recently, AGuIX nanoparticles, along with RT, have been entered a phase III clinical trial in the treatment of brain metastases [29]. Next, we chose melanoma as the object of study, and tested AGuIX nanoparticles radiosensitization effect on B16 cells. Reactive oxygen species (ROS) produced by RT was the key to eliminate cancer cells [30]. As shown in Figure 2A, the introduction of AGuIX nanoparticles could effectively amplify RT induced ROS generation. This is because AGuIX nanoparticles could produce photoelectrons and Auger electrons under radiation, which increased the

level of ROS in tumor cells, thus enhancing the biological effects of radiation. γ-H2AX is the earliest sensitive marker for DNA double-strand breaks, so the γ-H2AX antibody recognition immunofluorescence could be used as a reliable method to study radiation sensitivity [31]. The γ-H2AX immunofluorescence staining in Figure 2B demonstrated that AGuIX nanoparticles significantly cooperated with RT to induce more DNA double strand breaks, compared with the irradiation group alone. Clonogenic assays were used to detect the effect of AGuIX nanoparticles on the colony formation ability of B16 cells under 2, 4 and 6Gy radiation doses. After continuing to be cultured for 8-10 days, and clones were counted and the survival rate was plotted, as shown in Figure 2C. The survival rate of the B16 cells in the AGuIX nanoparticles group was lower, indicating that they were more sensitive to radiation. Then we analyzed the sensitizing enhancement ratios (SER), that is, the ratio of the required radiation dose alone to the dose of radiation combined with AGuIX nanoparticles on the premise of achieving the same specific biological effect. The calculated SER was ranging from 1.3 to 1.8, confirming that AGuIX nanoparticles had obvious radiosensitization effect. Finally, we also detected the apoptosis induced by AGuIX, and the results showed that apoptosis in AGuIX nanoparticles group increased significantly at 6 h (Figure S1) and 24 h (Figure 2D) after irradiation, which could develop early apoptosis into late apoptosis. Collectively, these results showed that AGuIX nanoparticles could increase radiation sensitization via enhancing radiation deposition and ROS production, then promoted cell apoptosis. All of these potentially indicated their improved therapeutic efficiency for *in vivo*.

Immunogenicity was enhanced by AGuIX nanoparticles.

Commonly, an appropriate dose of RT could also induce ICD, which was characterized by calcium reticulin (CRT) exposure, high mobility group box 1 protein (HMGB1) release and adenosine triphosphate (ATP) secretion [32, 33]. Therefore, the ICD induced by AGuIX nanoparticles was charactered *in vitro* and *in vivo*. As shown in Figure 3A, B16 cells treated with RT alone (6 Gy) presented very limited cell-surface exposure of CRT. However, when AGuIX nanoparticles were combined with RT (6 Gy), the synergistic effect resulted in more CRT exposure, which was also consistent with flow cytometry detection (Figure 3B). At the same time, we also detected in the cell culture supernatant that AGuIX-treated B16 tumor cells significantly released more HMGB-1 after irradiation (Figure 3C), indicating their superior capacity in inducing potent ICD.

Further, we evaluated the effect of AGuIX combined with RT on the CRT expression in B16 tumor-bearing mice. The tumors of irradiated mice were isolated, sectioned and stained with immunofluorescence. Tumors treated with AGuIX+RT represented more red fluorescence (Figure 3D), indicating that superior radiosensitization effect mediated by AGuIX also led to the high expression of CRT *in vivo*. Then we want to verify whether the exposed CRT could initiate immune response, and analyze the DCs in lymph nodes of irradiated mice by flow cytometry. The percentage of CD80$^+$CD86$^+$ mature DCs in AGuIX+RT group was significantly higher, compared to those treated with RT alone (Figure 3E). This indicated the ICD elicited by AGuIX nanoparticles could act as an immunogenic antigen, which was recognized, ingested, processed and presented by DCs. DCs were key molecules in initiating, regulating and maintaining

immune response. Therefore, it is inferred AGuIX nanoparticles has the potential to enhance ICD, activate DCs and induce systemic anti-tumor immune response.

Enhanced therapeutic efficacy on B16 bilateral tumor model.

In view of the excellent effect of AGuIX nanoparticles *in vitro* and *in vivo*, their antitumor efficacy investigation carried out in C57BL/6 mice with bilateral tumors. In the evaluation of reactive biomarkers, it was found that low-dose fractionated radiotherapy upregulated the expression of PD-L1 in tumor cells in mouse tumor model [34]. Combination RT and PD-1/PD-L1 signaling blocking could provide an immediate strategy for clinical evaluation to improve treatment efficiency. Therefore, anti-PD1 therapy was included in the subsequent treatment, which was expected to relieve the tumor immunosuppressive microenvironment caused by RT and enhance the activation of effector CD8$^+$ T cells in tumors. The B16-bearing mice were randomly divided into six groups, including saline, α-PD-1, RT, RT + α-PD-1, RT+AGuIX, and RT+AGuIX + α-PD-1. When the primary tumors volume reached 100–150 mm^3, mice were treated separately according to groups. The regimen for tumor inoculation, RT and PD-1 blockade was illustrated in Figure 4A. All treatments did not result in significant weight loss of animals (Figure S2), and no pathological changes of all tissues and organs were found in HE analysis (Figure S3). It showed that this combination therapy was feasible and its toxicity to the body could be negligible. Combination treatment of AGuIX-mediated RT and α-PD-1 antibody significantly inhibited the locally irradiated tumors, and the anti-tumor effect of RT combined with AGuIX nanoparticles was also better than that of RT alone (Figure 4B). The results showed that AGuIX did play a role in radiosensitization. More interestingly, when combined with the α-PD-1 antibody, AGuIX-mediated RT but also restrained distant, non-irradiated tumors (Figure 4C), indicating this combined therapy strategy provoked a systemic effective systemic antitumor immune response. Then we detected the immune response in tumor draining lymph nodes (DLNs) of mice. It was found that the percentage of CD4$^+$ and CD8$^+$ T cells in the combined treatment group was obviously up-regulated, which was the most direct manifestation of a strong anti-tumor immune response. The results of TUNEL detection in tumor sections confirmed t AGuIX-mediated RT caused local tumor apoptosis/necrosis, while a lower density of apoptotic tumor cells was observed in RT/α-PD-1 antibody treatment groups (Figure 4E). Tumor infiltrating CD8$^+$T cells (CD8$^+$TILs) were the strongest killers of tumor cells, which closely related to the survival rate of patients. In general, the expression of PD-1 in tumor tissues also increased with the increasing of CD8$^+$ TILs [35]. Immunohistochemistry (IHC) was implemented to further analyze the infiltration of CD8$^+$ T cells in tumor bed. CD8 immunohistochemical staining showed that AGuIX-mediated RT enhanced the recruitment and infiltration of CD8$^+$TILs, represented by brown cells. Combined with α-PD-1, the proportion of CD8$^+$TILs had significantly doubled, indicating that the introduction of α-PD-1 could weaken the exhaustion of CD8$^+$ T cells, so that the body always maintained a strong anti-tumor activity.

By detecting different types of immune cells in the primary tumor microenvironment and explaining their basic role in tumor growth and immune escape, that is, tumor immunoediting, to uncover their functions and molecular mechanisms, it is currently an important scientific problem in developing new treatment

methods to overcome cancer [36]. Flow cytometry analysis of T cells subsets in tumors showed that both RT+AGuIX and RT + α-PD-1 therapy effectively promoted the infiltration of effector CD8$^+$ T lymphocytes (Figure 5A&D), decreased number of CD4$^+$Foxp3$^+$ Treg cells (Figure 5B&E) and Gr-1$^+$ CD11b$^+$ MDSCs (Figure 5C&G) into tumor tissue, compared with the treatment of PBS, RT or α-PD-1. Furthermore, the combination immunotherapy (RT+AGuIX + α-PD-1) significantly increased the ratio of CD8$^+$ T cells to CD4$^+$Foxp3$^+$ Tregs (Figure 5F), which was implying an efficient infiltration of CD8$^+$ T cells and reverse of tumor immunosuppressive environment by introducing α-PD-1.

We further investigated how T cell immunity affected the efficacy of AGuIX-mediated RT plus α-PD-1 therapy, which was evaluated in a subcutaneous B16 tumor model. Mice were injected intraperitoneally with anti-CD4, anti-CD8, or mouse IgG antibodies to deplete CD4$^+$T or CD8$^+$T cells and then treated with AGuIX and RT combined with α-PD-1. The detailed experimental arrangement was shown in Figure 6A. Although AGuIX-mediated RT treatment was also given, the tumor growth of mice treated with anti-CD4 antibody and anti-CD8 antibody was rapid, and mice treated with IgG could significantly decrease tumor growth (Figure 6B&C). However, compared with the control group, the tumor growth in T cells depleting group still slowed down to a certain extent, which showed that AGuIX-mediated RT could induce DNA damage and promote ICD or apoptosis of tumor cells, thus leading to a mild anti-tumor effect. These were also consistent with the weight of the isolated primary and distant tumors (Figure 6D&E). These results suggest the antitumor efficacy of combined therapy was excessively dependent on both CD4$^+$ T and CD8$^+$ T cells, and further clarify the extensive and solid theoretical basis for using AGuIX-mediated RT to strengthen checkpoint blockade tumor immunotherapy.

Immunologic memory studies of AGuIX nanoparticles on pulmonary metastasis.

Efficient systemic immune response could be triggered by the AGuIX-mediated RT, and therefore we further studied its immunologic memory effect on established the pulmonary metastasis tumor model. Traditional tumor therapy such as radiotherapy only has a local therapeutic effect on in situ tumors, and the distal effect is not enough to control the metastasis of malignant tumors [37]. Different from traditional cancer therapy, immunotherapy aims to enhance the systemic immune response, in which activated cytotoxic T lymphocytes recognize and kill tumor cells to inhibit tumor metastasis. Briefly, B16 cells ($5×10^5$) were subcutaneously inoculated onto the right flanks (as the primary tumor), then B16 cells ($1×10^6$) were injected through tail vein. Subsequently, the mice received treatments according to the schedule given in Figure 7A. On the 30th day, mice were sacrificed and lung tissues of each group were collected for analysis. There was significant difference in the lung metastasis between untreated and treated groups. As shown in Figure 7B&C, AGuIX-mediated RT plus α-PD-1 combined treatment effectively decreased the locally irradiated tumors after irradiation. In comparison, RT, α-PD-1 and RT plus α-PD-1 groups showed only moderate anti-tumor efficacy. Compared with the single treatment group, the number of pulmonary nodules in the combined treatment group was negligible (Figure 7D). The results of H&E staining further confirmed AGuIX-mediated RT plus α-PD-1 effectively inhibited tumor metastasis. In Figure 7E, abnormal pathological structure and tumor tissue were observed in both the control group and

the single-treated group, while the lung tissue in the combined treatment group was close to the normal physiological structure. These results indicated the systemic antitumor immune response triggered by AGuIX-mediated RT plus α-PD-1efficiently inhibited tumor metastasis. Depending on the effective blocking of PD-1 pathway, AGuIX-mediated RT demonstrated a robust and powerful immunotherapy platform to prevent tumor metastasis.

Conlusions

In summary, a novel Gadolinium-based nanoparticle-AGuIX was designed for radioenhancer, which at low-dose RT could lead to tumor cell immunogenic cell death, including surface exposure of calreticulin, passive release of HMGB-1, and secreted ATP. Significantly, AGuIX-mediated RT activated the systemic immune response in vivo, which elicited powerful antitumor T-cell immunity and greatly promoted the infiltration of effector CD8$^+$ T cells in tumor. Moreover, the combination therapy strategy of AGuIX-mediated RT plus α-PD-1 checkpoint blockade produced a powerful immunotherapeutic effect by integrating the effective blocking of PD-1 pathway and inducing ICD as an in situ vaccine for primary tumors elimination, abscopal tumors suppression and pulmonary metastasis rejection. Taken together, the combination therapy strategy of AGuIX-mediated RT and α-PD-1 checkpoint blockade could amplify T cells immunity and relieve the immunosuppressive tumor environment, which is likely to be a promising comprehensive treatment strategy.

Methods

Materials.

Gadolinium chloride, tetraethyl orthosilicate and aminopropyltriethoxysilane were acquired from Aldrich Chemicals (France). Flow cytometry antibodies including CD16/32, CD3ε, CD4, CD8, Foxp3, Gr-1, CD11b, CD11c and CD86 were purchased from BioLegend (San Diego, CA, USA). Anti-Calreticulin antibody was purchased from Abcam (Cambridge, United Kingdom). The mouse regulatory T cell staining kit was obtained from eBioscience (San Diego, CA, USA). Mouse HMGB-1 ELISA kit was received from Beijing Solarbio Science & Technology Co., Ltd. (Beijing, China). The reactive oxygen species assay kit was purchased from Thermo Fisher Scientific (USA). The apoptosis detection kit was acquired from BD pharmingen (San Diego, CA, USA). Anti-CD4, anti-CD8, IgG and PD-1 antibodies were purchased from BioXCell, USA.

Cell lines and animals.

B16 tumor cells were purchased from the Cell Bank at the Chinese Academy of Sciences, supplied by ATCC. C57BL/6 mice were male, 6-8 weeks old, which were randomly assigned to either control group or experimental group.

Synthesis and characterization of AGuIX nanoparticles.

AGuIX nanoparticles were synthesized through the original top-down process described as follows: 1) forming Gd_2O_3 core; 2) entrapping in polysiloxane shell layer grafted with DOTAGA ligands; 3) dissolving Gd_2O_3 core due to DOTAGA ligands chelating Gd^{3+}; and 4) polysiloxane fracture [26]. The composition of the nanoparticles was determined by inductively coupled plasma mass spectrometry (ICP-MS), mass spectrometry, fluorescence spectroscopy, ^{29}Si solid-state NMR, ^1H NMR and diffusion ordered spectroscopy (DOSY). The dissolution of oxide core was confirmed by superconducting quantum interference device (SQUID) and electron paramagnetic resonance (EPR). The size and morphology of these nanoparticles were detected by photon correlation spectroscopy (PCS), transmission electron microscopy (TEM), respectively.

Clonogenic assay.

B16 cells were incubated in a 6-well plate with a density of 1000 cells per well for 24 h, then 1 mM ($[Gd^{3+}]$) of AGuIX nanoparticles were added one hour in advance, and then irradiated with 2, 4 and 6 Gy radiation doses. Then continue to culture for 8-10 days. Once colony formation was observed, discarded the culture medium. The plate was washed twice with PBS, and then stained with 0.5% w/v crystal violet solution. The survival percentage was calculated by the following formula: the number of irradiated colonies / the number of non-irradiated colonies.

Intracellular reactive oxygen species (ROS) measurements.

B16 cells were inoculated in 6-well plates for 24 h and treated with 1 mM ($[Gd^{3+}]$) of AGuIX nanoparticles for 1 h, then irradiated with 6 Gy. The intracellular ROS level was detected by ROS detection kit at 2 h and 4 h after radiation, according to the instructions.

Apoptosis/necrosis assay.

B16 cells were inoculated in 6-well plates for 24 h and treated with 1 mM ($[Gd^{3+}]$) of AGuIX nanoparticles for 1 h, then irradiated with 6 Gy. The cells were stained with FITC Annexin V apoptosis detection kit and quantified by flow cytometry at 6 h and 24 h after radiation.

DNA damage.

B16 cells were inoculated in 6-well plates for 24 h and treated with 1 mM ($[Gd^{3+}]$) of AGuIX nanoparticles for 1 h, then irradiated with 6 Gy. After incubation for 4 h, the cells were labled with phospho-Histone H2AX primary antibody and its corresponding secondary antibody for CLSM. ImageJ was used to count the number of cells with foci and number of foci in the nucleus.

Immunogenic cell death.

B16 cells were inoculated in 6-well plates for 24 h and treated with 1 mM ($[Gd^{3+}]$) of AGuIX nanoparticles for 1 h, then irradiated with 6 Gy. Four hours later, the cells were labeled with anti-Calreticulin (CRT)

antibody and detected by confocal microscope and flow cytometry respectively. Simultaneously, HMGB-1 secreted in the supernatant of cell culture was detected by ELISA.

Further, we evaluated the effect of AGuIX combined with RT on the immunogenic cell death in B16 tumor-bearing mice. The tumors of irradiated mice were isolated, sectioned and stained with anti-Calreticulin (CRT) antibody. To verify whether the exposed CRT could initiate immune response, we analyzed the DCs in lymph nodes of irradiated mice by flow cytometry, following the detailed steps described in the previous article [38, 39].

In vivo **anti-tumor efficacy on bilateral model.**

The primary and distal bilateral tumor model was established by subcutaneously inoculating 5×10^5 and 2×10^5 B16 cells into the right and left sides of C57BL/6 mice. The mice were randomly divided into six groups: Control, αPD-1, RT, RT+AGuIX, RT + αPD-1, RT+AGuIX + αPD-1. When the primary tumor volume reached $100-150$ mm^3, 1 mM ([Gd^{3+}]) AGuIX or PBS was injected into mice through tail vein. After injection 4h, mice were anesthetized and the primary tumors were irradiated with 4 Gy of Cr^{137} γ-ray at a dose rate of 1 Gy/min every 3 days for three times. Anti-PD1 antibody was injected intraperitoneally every 3 days at a dose of 100 μg/ mouse. The size of the tumors was measured with a caliper every day, in which the tumor volume was equal to (width^2 × length)/2. Each mouse was weighed every day to assess the toxicity. Mice were sacrificed on the 30th day.

The tumors were isolated and incubated with 1 mg/ml collagenase I at 37°C for 1 hour. Then the tumor single-cell suspension was prepared by filtering through a 40 μ m cell stainer. The tumor-draining lymph nodes were collected, ground and filtered. The single-cell suspension was first blocked with anti-CD16/32, and then classified and labeled with the following flow cytometry antibodies: CD3ε, CD4, CD8, Foxp3, Gr-1, CD11b, CD11c, and CD86. Finally, the proportion of all kinds of cells was analyzed by flow cytometry, and the data were processed by Flow Jo software.

T cells depletion.

As mentioned above, bilateral subcutaneous models were established to observe the anti-tumor effect *in vivo*. When the primary tumor volume reached $100-150$ mm^3, 1 mM ([Gd^{3+}]) AGuIX or PBS were injected into mice by tail vein. Anti-CD4, anti-CD8, or mouse IgG antibodies were injected intraperitoneally at a dose of 200 μg per mouse on -2, 0, 4 and 8 days. Mice were anesthetized and only the primary tumors were treated with RT in accordance with the previous regimen. In order to evaluate the effect of treatment, the tumors growth and body weight were monitored daily.

In vivo **anti-tumor efficacy on pulmonary metastasis model.**

The right flanks of 6-8-week-old C57BL/6 mice (18-20g) were subcutaneously inoculated with B16 cells (5×10^5) as primary tumors. When the primary tumors reached about 100 mm^3, B16 cells (1×10^6) were injected into the tail vein to establish the pulmonary metastasis model. One day later, the mice were

randomly divided into 6 groups (n =6). The mice were injected intravenously with 1 mM ([Gd^{3+}]) AGuIX or PBS. After injection of 4h, mice were anesthetized and only the primary tumors were treated with RT in accordance with the previous regimen. Anti-PD1 antibody was injected intraperitoneally every 3 days at a dose of 100 μg/ mouse. Mice were sacrificed on the 30th day and the lung tissues of different treatment groups were collected and photographed. In addition, H&E staining of lung tissues was also implemented to identify the metastatic tumors. Lungs were fixed in 4% paraformaldehyde solution for 12 h, and then dehydrated and embedded in paraffin, and finally sectioned and stained by hematoxylin and eosin. The slice thickness was 5 μm. The metastasis lesions in lungs were counted by observation to assess the anti-metastasis effect.

Statistical analysis

All animal studies were performed in randomization and data were analyzed multiple comparisons where there were more than two groups being compared, or where data was collected over time by one-way ANOVA in Prism 7 (GraphPad Software, Inc., La Jolla, CA, USA). P<0.05 was considered to be statistically significant. All values are presented as means ± SDs, unless indicated otherwise.

Declarations

Ethics approval and consent to participate

All animal feeding and experimental procedures were conducted in accordance with the rules established by Animal Experiment Ethics Committee and Authority of Institute of Radiation Medicine, Chinese Academy of Medical Sciences (Approval No: SYXK (Jin) 2019-0002).

Consent for publication

All authors agree with the submission and publication.

Availability of data and materials

The data supporting the findings of this study are available within this paper and Additional files. Additional data can also be available from the corresponding author on reasonable request.

Competing interests

The authors declare no competing financial interest.

Funding

Authors' contributions

Huijuan Song: Conceptualization, Methodology, Writing - Original Draft; Ningning He: Software; Chang Xu: Software; Yan Wang: Funding acquisition; Liqing Du: Methodology; Yang Liu: Validation; Qin Wang: Validation; Kaihua Ji: Methodology; Jinhan Wang: Investigation; Manman Zhang: Investigation; Yeqing Gu: Formal analysis; Yumin Zhang: Writing - Review & Editing; Weiwei Wang: Supervision; Olivier Tillement: Supervision; Li Feng: Funding acquisition; Qiang Liu: Project administration, Writing - Review & Editing

References

1. Allen C, Her S and Jaffray DA. Radiotherapy for Cancer: Present and Future. Adv Drug Deliv Rev. 2017;109:1–2.

2. Citrin DE. Recent Developments in Radiotherapy. N Engl J Med. 2017;377:1065–1075.

3. Scully R, Panday A, Elango R and Willis NA. DNA double-strand break repair-pathway choice in somatic mammalian cells. Nat Rev Mol Cell Biol. 2019;20:698–714.

4. Buckley AM, Lynam-Lennon N, O'Neill H and O'Sullivan J. Targeting hallmarks of cancer to enhance radiosensitivity in gastrointestinal cancers. Nat Rev Gastroenterol Hepatol. 2020;17:298–313.

5. McLaughlin M, Patin EC, Pedersen M, Wilkins A, Dillon MT, Melcher AA and Harrington KJ. Inflammatory microenvironment remodelling by tumour cells after radiotherapy. Nat Rev Cancer. 2020;20:203–217.

6. Weichselbaum RR, Liang H, Deng L and Fu YX. Radiotherapy and immunotherapy: a beneficial liaison? Nat Rev Clin Oncol. 2017;14:365–379.

7. Rodríguez-Ruiz ME, Vanpouille-Box C, Melero I, Formenti SC and Demaria S. Immunological Mechanisms Responsible for Radiation-Induced Abscopal Effect. Trends in immunology. 2018;39:644–655.

8. Wan C, Sun Y, Tian Y, Lu L, Dai X, Meng J, Huang J, He Q, Wu B, Zhang Z, Jiang K, Hu D, Wu G, Lovell JF, Jin H and Yang K. Irradiated tumor cell-derived microparticles mediate tumor eradication via cell killing and immune reprogramming. Sci Adv. 2020;6:eaay9789.

9. Tesniere A, Panaretakis T, Kepp O, Apetoh L, Ghiringhelli F, Zitvogel L and Kroemer G. Molecular characteristics of immunogenic cancer cell death. Cell Death Differ. 2008;15:3–12.

10. Bronte V. Tumors STING adaptive antitumor immunity. Immunity. 2014;41:679–81.

11. Akkari L, Bowman RL, Tessier J, Klemm F, Handgraaf SM, de Groot M, Quail DF, Tillard L, Gadiot J, Huse JT, Brandsma D, Westerga J, Watts C and Joyce JA. Dynamic changes in glioma macrophage

populations after radiotherapy reveal CSF-1R inhibition as a strategy to overcome resistance. Sci Transl Med. 2020;12.

12. Jiang W, Chan CK, Weissman IL, Kim BYS and Hahn SM. Immune Priming of the Tumor Microenvironment by Radiation. Trends Cancer. 2016;2:638–645.

13. Liu YT and Sun ZJ. Turning cold tumors into hot tumors by improving T-cell infiltration. Theranostics. 2021;11:5365–5386.

14. Portella L and Scala S. Ionizing radiation effects on the tumor microenvironment. Semin Oncol. 2019;46:254–260.

15. Liu Y, Zhang P, Li F, Jin X, Li J, Chen W and Li Q. Metal-based NanoEnhancers for Future Radiotherapy: Radiosensitizing and Synergistic Effects on Tumor Cells. Theranostics. 2018;8:1824–1849.

16. Bort G, Lux F, Dufort S, Crémillieux Y, Verry C and Tillement O. EPR-mediated tumor targeting using ultrasmall-hybrid nanoparticles: From animal to human with theranostic AGuIX nanoparticles. Theranostics. 2020;10:1319–1331.

17. Du Y, Sun H, Lux F, Xie Y, Du L, Xu C, Zhang H, He N, Wang J, Liu Y, Leduc G, Doussineau T, Ji K, Wang Q, Lin Z, Wang Y, Liu Q and Tillement O. Radiosensitization Effect of AGuIX, a Gadolinium-Based Nanoparticle, in Nonsmall Cell Lung Cancer. ACS applied materials & interfaces. 2020;12:56874–56885.

18. Verry C, Dufort S, Villa J, Gavard M, Iriart C, Grand S, Charles J, Chovelon B, Cracowski JL, Quesada JL, Mendoza C, Sancey L, Lehmann A, Jover F, Giraud JY, Lux F, Crémillieux Y, McMahon S, Pauwels PJ, Cagney D, Berbeco R, Aizer A, Deutsch E, Loeffler M, Le Duc G, Tillement O and Balosso J. Theranostic AGuIX nanoparticles as radiosensitizer: A phase I, dose-escalation study in patients with multiple brain metastases (NANO-RAD trial). Radiother Oncol. 2021;160:159–165.

19. de Miguel M and Calvo E. Clinical Challenges of Immune Checkpoint Inhibitors. Cancer Cell. 2020;38:326–333.

20. Bagchi S, Yuan R and Engleman EG. Immune Checkpoint Inhibitors for the Treatment of Cancer: Clinical Impact and Mechanisms of Response and Resistance. Annu Rev Pathol. 2021;16:223–249.

21. Galluzzi L, Humeau J, Buqué A, Zitvogel L and Kroemer G. Immunostimulation with chemotherapy in the era of immune checkpoint inhibitors. Nat Rev Clin Oncol. 2020;17:725–741.

22. Sheng H, Huang Y, Xiao Y, Zhu Z, Shen M, Zhou P, Guo Z, Wang J, Wang H, Dai W, Zhang W, Sun J and Cao C. ATR inhibitor AZD6738 enhances the antitumor activity of radiotherapy and immune checkpoint inhibitors by potentiating the tumor immune microenvironment in hepatocellular carcinoma. J Immunother Cancer. 2020;8.

23. Liang H, Deng L, Hou Y, Meng X, Huang X, Rao E, Zheng W, Mauceri H, Mack M, Xu M, Fu YX and Weichselbaum RR. Host STING-dependent MDSC mobilization drives extrinsic radiation resistance. Nat Commun. 2017;8:1736.

24. Le Duc G, Miladi I, Alric C, Mowat P, Bräuer-Krisch E, Bouchet A, Khalil E, Billotey C, Janier M, Lux F, Epicier T, Perriat P, Roux S and Tillement O. Toward an image-guided microbeam radiation therapy

using gadolinium-based nanoparticles. ACS nano. 2011;5:9566–74.

25. Sancey L, Lux F, Kotb S, Roux S, Dufort S, Bianchi A, Crémillieux Y, Fries P, Coll JL, Rodriguez-Lafrasse C, Janier M, Dutreix M, Barberi-Heyob M, Boschetti F, Denat F, Louis C, Porcel E, Lacombe S, Le Duc G, Deutsch E, Perfettini JL, Detappe A, Verry C, Berbeco R, Butterworth KT, McMahon SJ, Prise KM, Perriat P and Tillement O. The use of theranostic gadolinium-based nanoprobes to improve radiotherapy efficacy. The British journal of radiology. 2014;87:20140134.

26. Mignot A, Truillet C, Lux F, Sancey L, Louis C, Denat F, Boschetti F, Bocher L, Gloter A, Stéphan O, Antoine R, Dugourd P, Luneau D, Novitchi G, Figueiredo LC, de Morais PC, Bonneviot L, Albela B, Ribot F, Van Lokeren L, Déchamps-Olivier I, Chuburu F, Lemercier G, Villiers C, Marche PN, Le Duc G, Roux S, Tillement O and Perriat P. A top-down synthesis route to ultrasmall multifunctional Gd-based silica nanoparticles for theranostic applications. Chemistry (Weinheim an der Bergstrasse, Germany). 2013;19:6122–36.

27. Burns AA, Vider J, Ow H, Herz E, Penate-Medina O, Baumgart M, Larson SM, Wiesner U and Bradbury M. Fluorescent silica nanoparticles with efficient urinary excretion for nanomedicine. Nano letters. 2009;9:442–8.

28. Smith MC, Crist RM, Clogston JD and McNeil SE. Zeta potential: a case study of cationic, anionic, and neutral liposomes. Anal Bioanal Chem. 2017;409:5779–5787.

29. Verry C, Sancey L, Dufort S, Le Duc G, Mendoza C, Lux F, Grand S, Arnaud J, Quesada JL, Villa J, Tillement O and Balosso J. Treatment of multiple brain metastases using gadolinium nanoparticles and radiotherapy: NANO-RAD, a phase I study protocol. BMJ Open. 2019;9:e023591.

30. Choi BJ, Jung KO, Graves EE and Pratx G. A gold nanoparticle system for the enhancement of radiotherapy and simultaneous monitoring of reactive-oxygen-species formation. Nanotechnology. 2018;29:504001.

31. Kinner A, Wu W, Staudt C and Iliakis G. Gamma-H2AX in recognition and signaling of DNA double-strand breaks in the context of chromatin. Nucleic Acids Res. 2008;36:5678–94.

32. Duan X, Chan C and Lin W. Nanoparticle-Mediated Immunogenic Cell Death Enables and Potentiates Cancer Immunotherapy. Angew Chem Int Ed Engl. 2019;58:670–680.

33. Ni K, Luo T, Culbert A, Kaufmann M, Jiang X and Lin W. Nanoscale Metal-Organic Framework Co-delivers TLR-7 Agonists and Anti-CD47 Antibodies to Modulate Macrophages and Orchestrate Cancer Immunotherapy. Journal of the American Chemical Society. 2020;142:12579–12584.

34. Dovedi SJ, Adlard AL, Lipowska-Bhalla G, McKenna C, Jones S, Cheadle EJ, Stratford IJ, Poon E, Morrow M, Stewart R, Jones H, Wilkinson RW, Honeychurch J and Illidge TM. Acquired resistance to fractionated radiotherapy can be overcome by concurrent PD-L1 blockade. Cancer research. 2014;74:5458–68.

35. Jansen CS, Prokhnevska N, Master VA, Sanda MG, Carlisle JW, Bilen MA, Cardenas M, Wilkinson S, Lake R, Sowalsky AG, Valanparambil RM, Hudson WH, McGuire D, Melnick K, Khan AI, Kim K, Chang YM, Kim A, Filson CP, Alemozaffar M, Osunkoya AO, Mullane P, Ellis C, Akondy R, Im SJ, Kamphorst

AO, Reyes A, Liu Y and Kissick H. An intra-tumoral niche maintains and differentiates stem-like CD8 T cells. Nature. 2019;576:465–470.

36. O'Donnell JS, Teng MWL and Smyth MJ. Cancer immunoediting and resistance to T cell-based immunotherapy. Nat Rev Clin Oncol. 2019;16:151–167.

37. Ngwa W, Irabor OC, Schoenfeld JD, Hesser J, Demaria S and Formenti SC. Using immunotherapy to boost the abscopal effect. Nature reviews Cancer. 2018;18:313–322.

38. Song H, Yang P, Huang P, Zhang C, Kong D and Wang W. Injectable polypeptide hydrogel-based co-delivery of vaccine and immune checkpoint inhibitors improves tumor immunotherapy. Theranostics. 2019;9:2299–2314.

39. Song H, Huang P, Niu J, Shi G, Zhang C, Kong D and Wang W. Injectable polypeptide hydrogel for dual-delivery of antigen and TLR3 agonist to modulate dendritic cells in vivo and enhance potent cytotoxic T-lymphocyte response against melanoma. Biomaterials. 2018;159:119–129.

Scheme

Scheme 1 is available in the Supplemental Files Section.
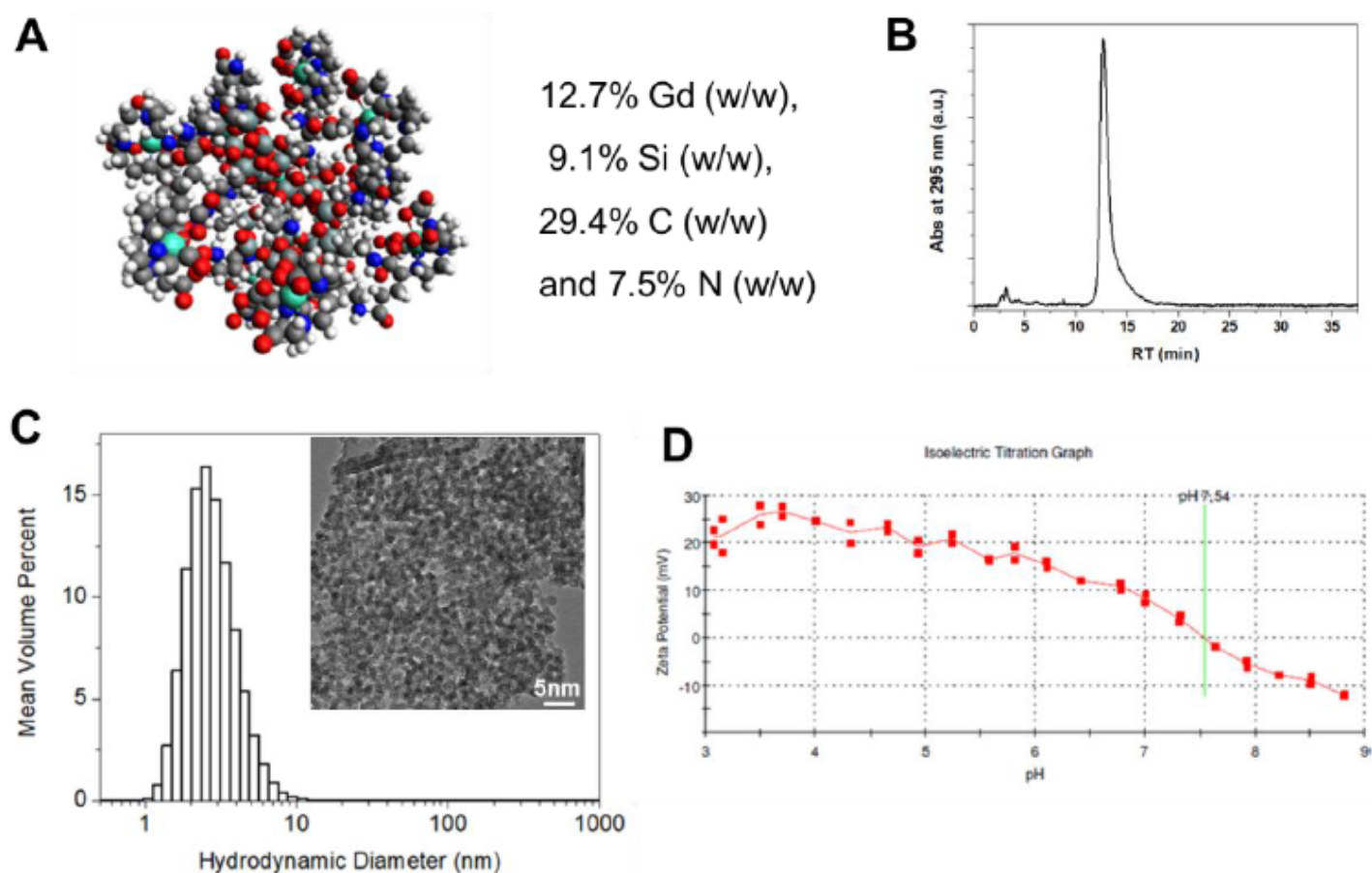
Figures

Page 16/23

Figure 1

Physicochemical characterization of AGuIX nanoparticles. (A) The three-dimensional structure and element composition of AGuIX nanoparticles. Gadolinium atoms were represented by green, silicon atoms by pale grey, carbon atoms by grey, nitrogen atoms by blue, oxygen atoms by red, and hydrogen atoms by white. AGuIX were composed of 12.7% Gd (w/w), 9.1% Si (w/w), 29.4% C (w/w) and 7.5% N (w/w). (B) HPLC measurement of AGuIX nanoparticles (detection at 295 nm). (C) Volume weighed particle size distribution of AGuIX nanoparticles by dynamic light scattering. The inset shows the HRTEM of the corresponding particle. (D) Zeta potential of AGuIX nanoparticles as a function of pH through electrophoretic light scattering.
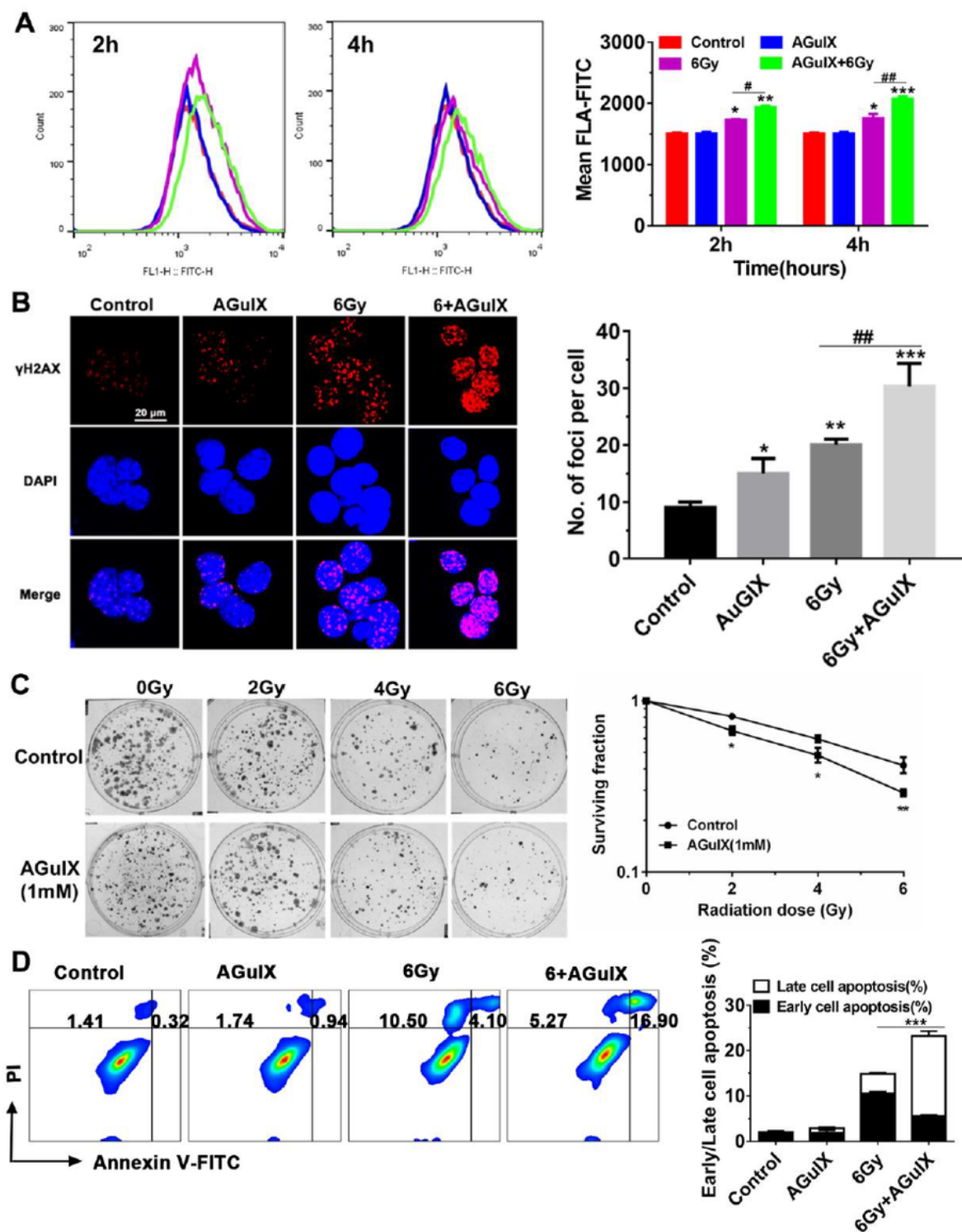
Figure 2

The increased radiosensitivity and mechanistic studies of AGuIX nanoparticles on B16 cells in vitro. (A) The ionizing radiation-induced ROS levels and total fluorescence intensity of each group detected by flow cytometry. (B) Representation of γH2AX foci formation in B16 cells of each group and the number of γH2AX foci in each B16 cell after irradiation (C) Representation of colony formation stained with crystal violet solution and calculation of surviving fraction. (D) Representative flow cytometry data plot and

qualitative proportion of early and late cell apoptosis in Annexin V/PI apoptosis analysis of B16 cells. *P ≤ 0.05, **P ≤ 0.01, and ***P ≤ 0.001, versus the control; #P < 0.05 and ##P < 0.01, between the indicated groups.
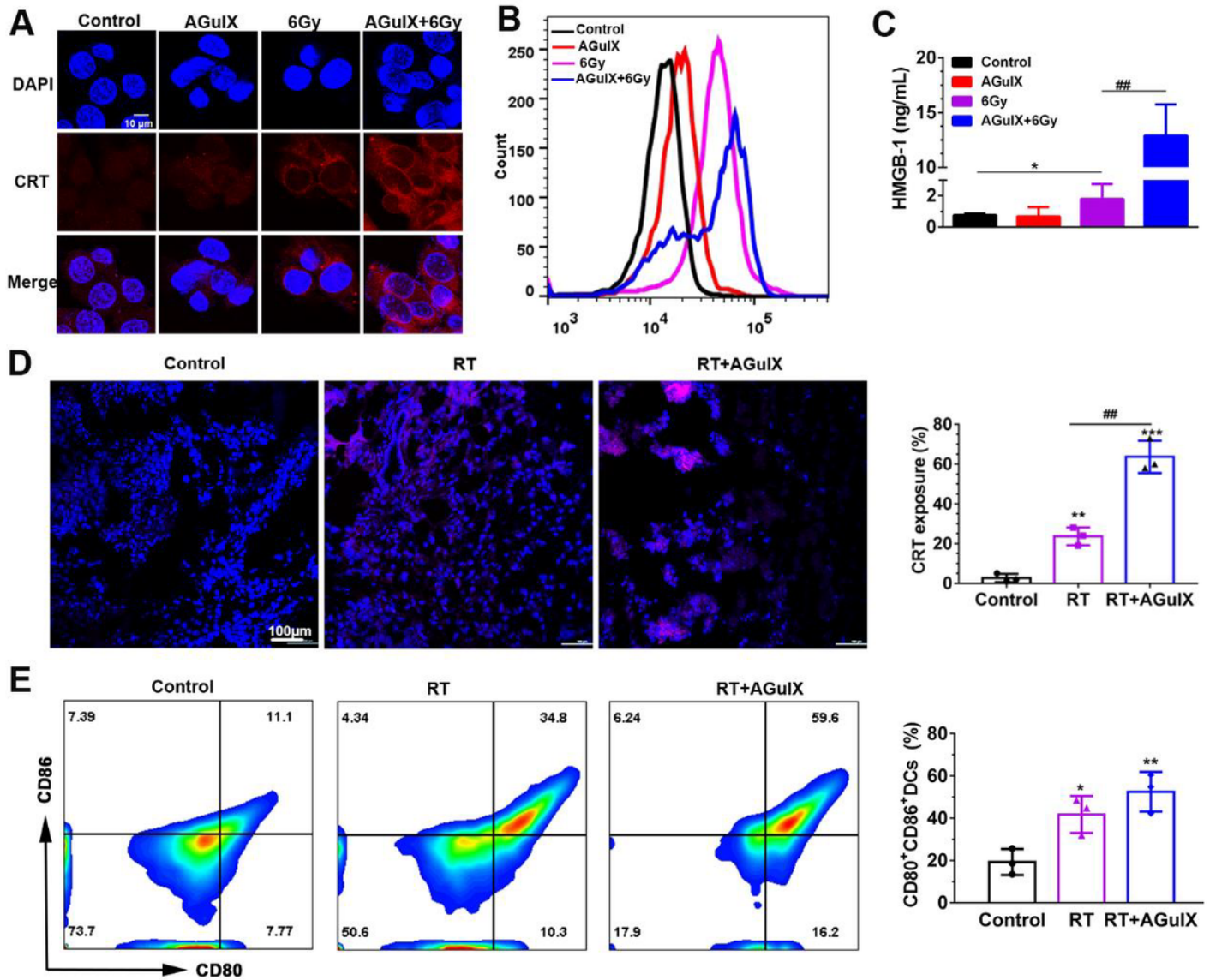

Figure 3

Immunogenic cell death detection *in vitro* and *in vivo*. (A) CRT exposure on B16 cells treated with AGuIX and radiation. (B) Quantitative analysis of CRT exposure on B16 cells by flow cytometry. (C) The secretion of HMGB-1 in culture medium after different treatments. (D) In vivo CRT expression on tumor slides of B16 tumor-bearing mice. Relative percentages of the CRT exposure in tumor tissues of mice in different treatment groups. (E) Representative flow cytometry data plot and proportion of mature DCs in lymph nodes of B16 tumor-bearing mice in different treatment groups. (n = 3 independent replicates). *P ≤ 0.05, **P ≤ 0.01, and ***P ≤ 0.001, versus the control; ##P < 0.01, between the indicated groups.
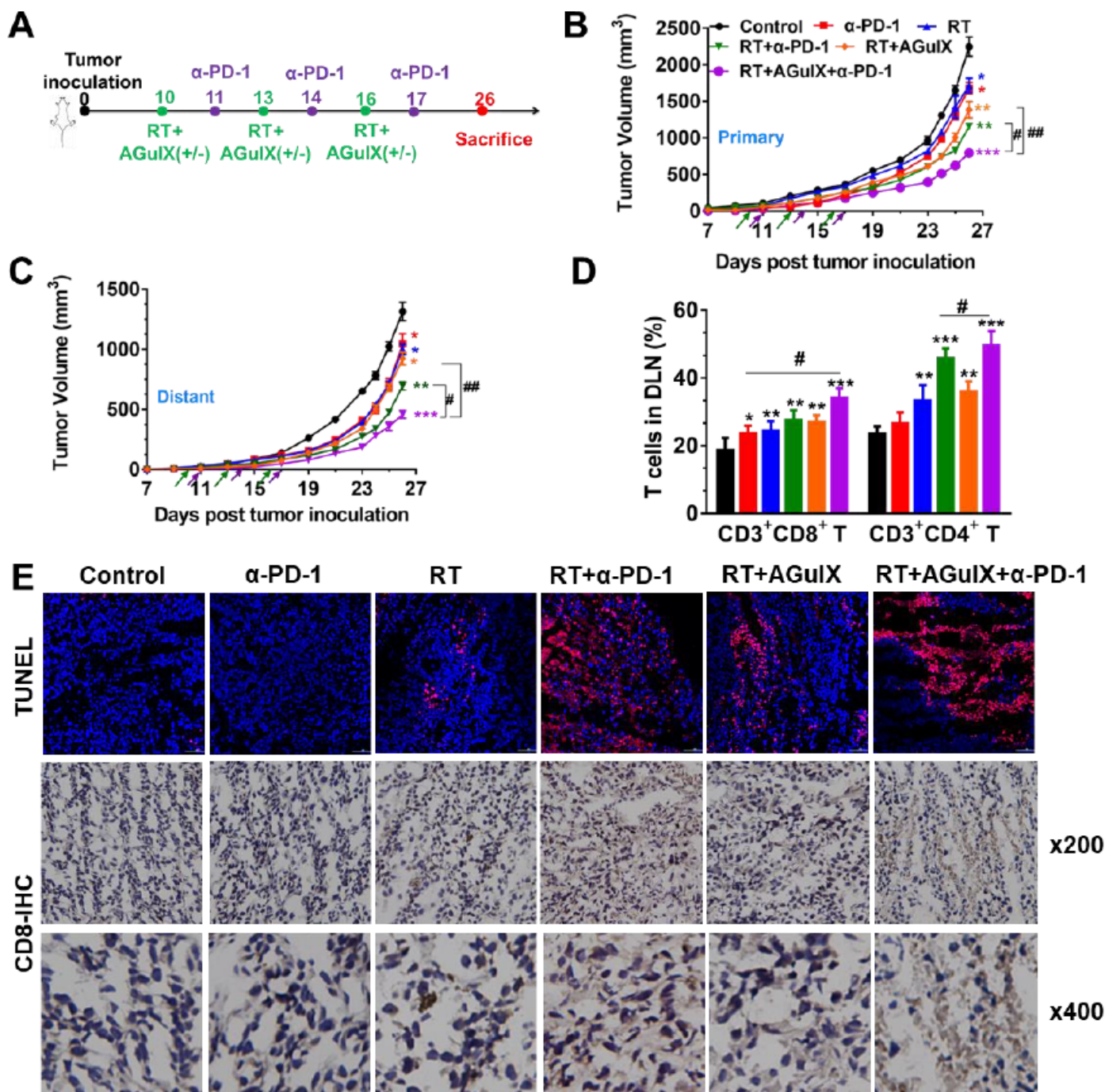
Figure 4

Antitumor efficiency of AGuIX nanoparticles and αPD-1 in B16 tumor-bearing mice. (A) Schematic diagram of experimental design for systemic immune response study. (B) Average growth curves for left and right (C) tumors in mice. (D) The percentage of CD3$^+$CD8$^+$ and CD3$^+$CD4$^+$ T cells in DLNs. (E) Histological examination of tumor slices for TUNEL and CD8 expression after various treatments. Data are given as means ± SD (n = 5 to 10). *P ≤ 0.05, **P ≤ 0.01, and ***P ≤ 0.001, versus the control; #P < 0.05 and ##P < 0.01, between the indicated groups.
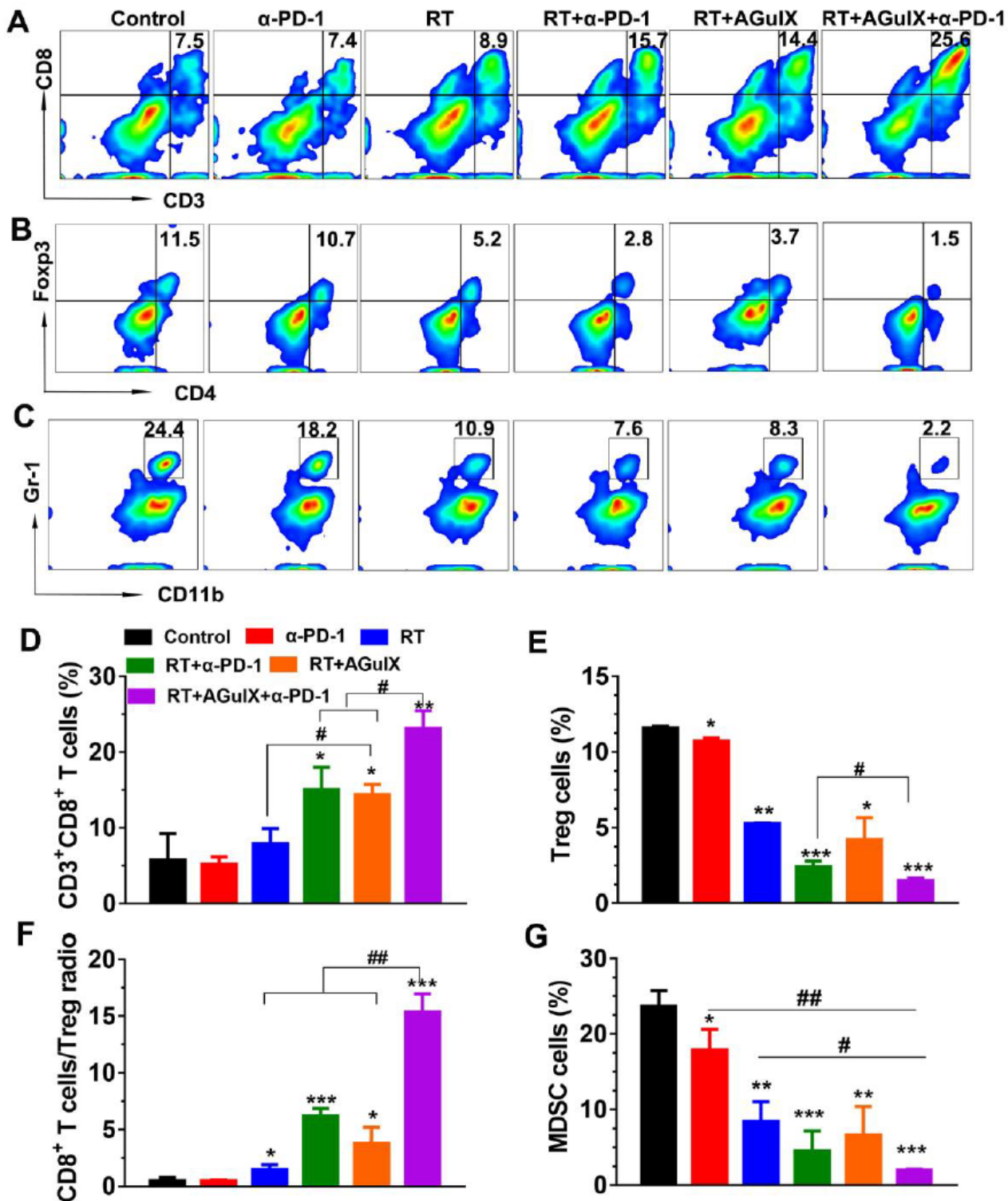
Figure 5

Tregs and MDSCs suppression and immune microenvironment relive induced by AGuIX nanoparticles and αPD-1 in B16 tumor-bearing mice. (A) Representative flow cytometry profiles of CD3$^+$CD8$^+$ T cells, CD4$^+$ Foxp3$^+$ Treg cells (B), and Gr-1$^+$ CD11b$^+$ MDSCs (C) infiltrated in tumors. (D) Quantitative analysis of the proportion of tumor infiltrating CD3$^+$CD8$^+$ T cells, and Tregs in CD4$^+$ T cells (E). (F) Ratio of CD8$^+$ T

cells to Tregs in the tumors. (G) Percentage of Gr-1$^+$ CD11b$^+$ MDSCs in the tumors. Data represents mean ± SDs (n = 5). *P <0.05, **P < 0.01 and ***P < 0.001, versus the control; $^\#$P < 0.05 and $^{\#\#}$P < 0.01, between the indicated groups.
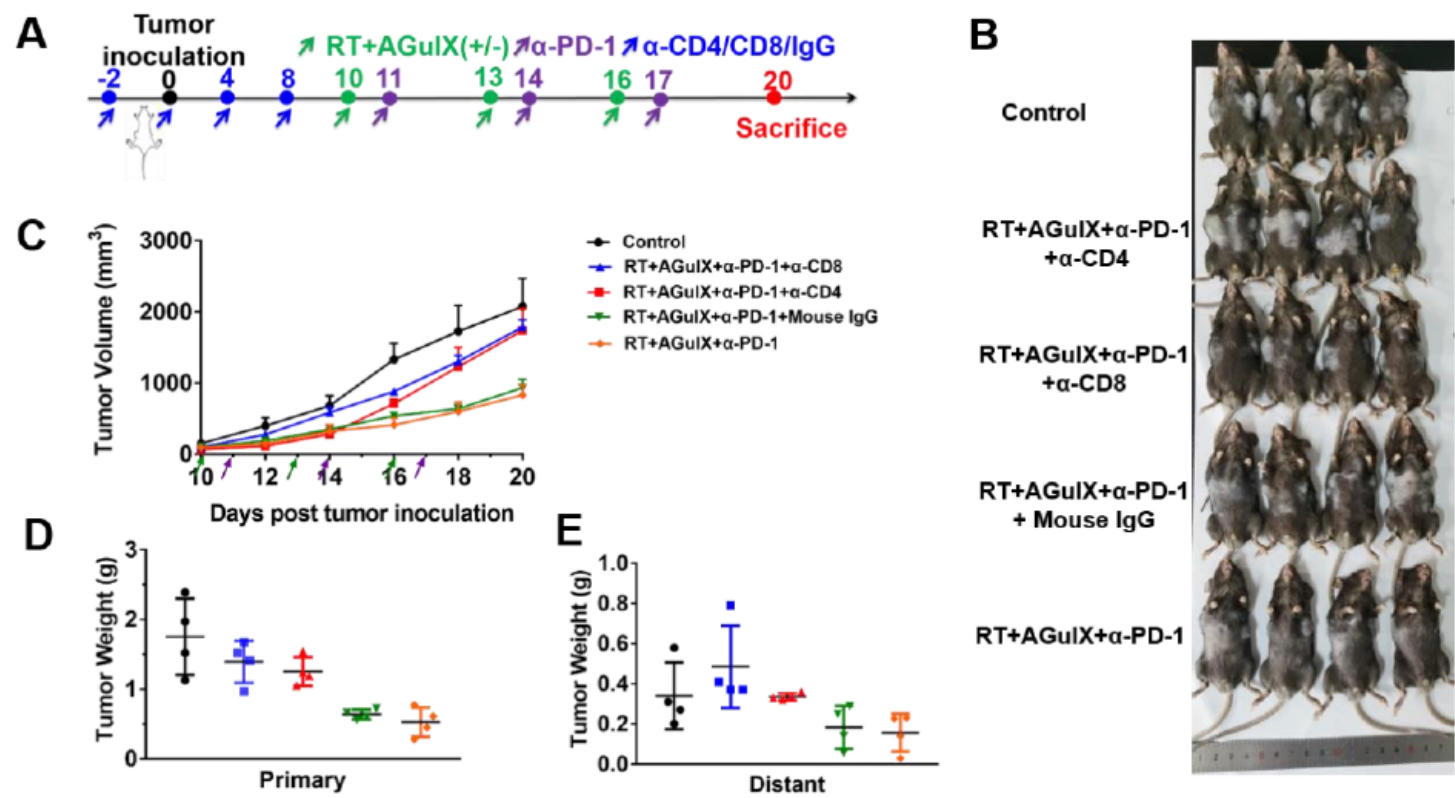

Figure 6

Tumor growth of B16 tumor-bearing mice after T cell depletion and treated with AGuIX nanoparticles, αPD-1 and irradiation. (A) Schedule of administration and treatment. (B) Tumor photographs of the tumor-bearing mice at the end of the experiment. (C) Tumor growth curves of tumor-bearing mice following therapy. (D) Tumor weight for left and right (E) isolated from tumor-bearing mice.
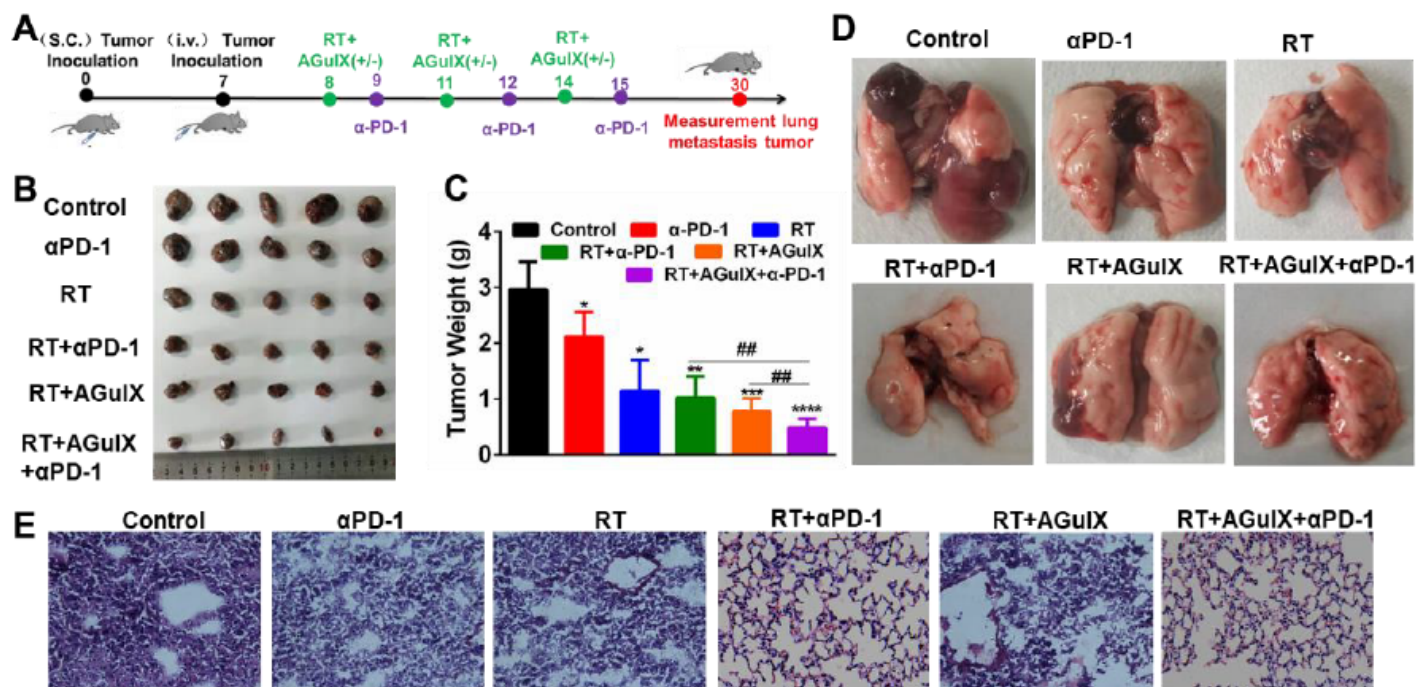
Figure 7

Anti-metastatic effect of AGuIX NPs in the pulmonary metastasis experiment. (A) Schedule of in vivo administration and treatment. (B) Tumor photographs and tumor weight (C) for primary tumors isolated from tumor-bearing mice at the end of the experiment. (D) Photographs of lung metastic nodules (n=5). (E) H&E staining of lung tissue from mice with different treatments. *P ≤ 0.05, **P ≤ 0.01, and ***P ≤ 0.001, versus the control; #P < 0.05 and ##P < 0.01, between the indicated groups.

Supplementary Files

This is a list of supplementary files associated with this preprint. Click to download.

- abstract.docx
- Scheme1.png
- supportinginformation913.docx